Inorganic Chemistry

Article

pubs.acs.org/IC

New BDH-TTP/$[M^{III}(C_5O_5)_3]^{3-}$ (M = Fe, Ga) Isostructural Molecular Metals

Luca Pilia,[†,‡] Elisa Sessini,[†] Flavia Artizzu,[†] Masahiro Yamashita,[§] Angela Serpe,[†] Kazuya Kubo,[§] Hiroshi Ito,[▽] Hisaaki Tanaka,[▽] Shin-ichi Kuroda,[▽] Jun-ichi Yamada,[⊥] Paola Deplano,[†] Carlos J. Gómez-García,[∥] and Maria Laura Mercuri*[,†]

[†]Dipartimento di Scienze Chimiche e Geologiche, Università degli Studi di Cagliari, S.S. 554 – Bivio per Sestu, I09042 Monserrato (Cagliari), Italy

[‡]EaStChem and School of Chemistry, University of Edinburgh, King's Buildings, West Mains Road, Edinburgh EH9 3JJ, United Kingdom

[§]Department of Chemistry, Tohoku University, Sendai 980-8578, Japan

[▽]Department of Applied Physics, Nagoya University, Nagoya 464-8603, Japan

[⊥]Department of Material Science, University of Hyogo, 3-2-1 Kouto, Kamigori-cho, Ako-gun, Hyogo 678-1297, Japan

[∥]Instituto de Ciencia Molecular (ICMol), Parque Científico, Universidad de Valencia, C/Catedrático José Beltrán, 2, 46980 Paterna (Valencia), Spain

Supporting Information

ABSTRACT: Two new isostructural molecular metals—(BDH-TTP)$_6[M^{III}(C_5O_5)_3]\cdot CH_2Cl_2$ (BDH-TTP = 2,5-bis(1,3-dithiolan-2-ylidene)-1,3,4,6-tetrathiapentalene, where M = Fe (**1**) and Ga (**2**))—have been prepared and fully characterized. Compound **1** is a molecular conductor showing paramagnetic behavior, which is due to the presence of isolated $[Fe(C_5O_5)_3]^{3-}$ complexes with high-spin $S = {}^5/_2$ Fe(III) metal ions. The conductivity originates from the BDH-TTP organic donors arranged in a κ-type molecular packing. At 4 kbar, compound **1** behaves as a metal down to ∼100 K, showing high conductivity (∼10 S cm^{-1}) at room temperature. When applying a pressure higher than 7 kbar, the metal–insulator (M-I) transition is suppressed and the compound retains the metallic state down to low temperatures (2 K). For **1**, ESR signals have been interpreted as being caused by the fine structure splitting of the high-spin ($S = {}^5/_2$) state of Fe(III) in the distorted octahedral crystal field from the ligands. At 4 kbar, the isostructural compound **2** behaves as a metal down to ∼100 K, although it is noteworthy that the M-I transition is not suppressed, even at pressures of 15 kbar. For **2**, only the signal assigned to delocalized π-electrons has been observed in the ESR measurements.

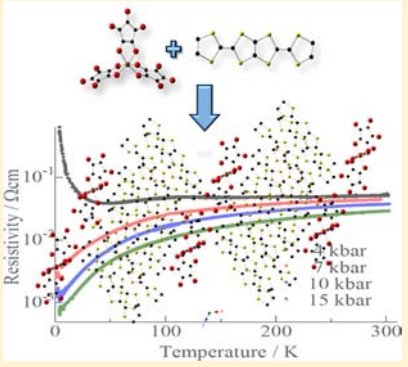

INTRODUCTION

The development of π-d systems as multifunctional materials represents one of the main targets in current materials science for their potential applications for future molecular electronics.[1] Since the discovery of coexistence of localized electrons and metallic conductivity in the charge transfer salt, (BEDT-TTF)$_3[CuCl_4]\cdot H_2O$ (BEDT-TTF = bis(ethylenedithio)-tetrathiafulvalene),[2] much effort has been devoted to prepare and physically characterize this type of multifunctional molecule-based materials. The aim was to investigate if metallic conductivity can stabilize indirect exchange interactions among the localized magnetic moments mediated by the conducting electrons. Several organic radicals of the tetrathiafulvalene (TTF) family, well-known for being the largest family of organic (super)conductors, were used as building blocks for such hybrid molecular conductors, in combination with magnetic metal transition complexes of different sizes and geometries.[1] Despite the large number of radical salts so far prepared, most of them do not present any indirect interaction between the paramagnetic centers, since they are semiconductors.[1] Furthermore, among the few metallic paramagnetic salts, this type of interaction has only been observed in very few cases.[3,4] (BET-TTF)$_2[FeCl_4]$ (BET-TTF = bis(ethylenethio) tetrathiafulvalene), which is metallic from room temperature down to 20 K and displays a weak, although noticeable, antiferromagnetic coupling between the Fe(III) ions, is one of these rare examples.[3] It is also noteworthy the compound λ-(BETS)$_2[(FeCl_4)]$ (BETS = bis(ethylenedithio)-tetraselenafulvalene) that shows a metallic behavior down to 8 K, where a M-I transition occurs.[5] Applying a magnetic field higher than 10 T, the M-I transition is suppressed and, particularly, for a range of magnetic field in the range 18 - 41 T, it behaves as a superconductor.[5] Using the octahedral

Received: October 12, 2012
Published: December 17, 2012

   dx.doi.org/10.1021/ic302234j | Inorg. Chem. 2013, 52, 423–430

$[M(ox)_3]^{3-}$ (ox = oxalato = $C_2O_4^{2-}$) complexes, Day et al. obtained the series $(BEDT\text{-}TTF)_4[A^IM^{III}(ox)_3]\cdot$solvent (BEDT-TTF = bis(ethylenedithio) tetrathiafulvalene); A = H_3O^+, K^+ and NH_4^+; M = Cr, Fe, Co, Ga, and Al; solvent = C_6H_5CN, $C_6H_5NO_2$, C_5H_5N, and CH_2Cl_2).[1] In these series, recently enlarged with PhX (X = F, Cl, Br, and I) as solvents for M = Cr and Fe,[6] up to 13 paramagnetic superconductors with critical temperatures ranging from 1.0 K to 8.5 K have been reported.[1,6] Day et al. have clearly demonstrated that the transport properties are related to structural changes and/or small changes of the components of these salts. Recently, some of us have successfully explored the substitution of the chelating ligand coordinated to the metal(III) ion in the metal transition complexes. Two new dual-function materials α-$(BEDT\text{-}TTF)_5[Fe(C_5O_5)_3]\cdot 5H_2O$ and β''-$(BEDT\text{-}TTF)_5[Fe(C_5O_5)_3]\cdot C_6H_5CN$, containing the new paramagnetic $[Fe(C_5O_5)_3]^{3-}$ ($C_5O_5^{2-}$ = croconate, dianion of croconic acid = 4,5-dihydroxycyclopent-4-ene-1,2,3-trione) anion have been obtained.[7] This anion contains the croconato ligand whose coordination modes and ability to mediate magnetic interactions[8−12] are very similar to those of the oxalate one.

The structure of both compounds consists of alternating layers of BEDT-TTF molecules separated by layers of $[Fe(C_5O_5)_3]^{3-}$ anions and solvent molecules (H_2O or C_6H_5CN). The BEDT-TTF molecules in the compound with H_2O are arranged in a herringbone packing motif, typical of the α-phase, which is induced by the chirality of the anions, since the twisting of the BEDT-TTF molecules is directed by the spatial orientation of the $[C_5O_5]^{2-}$ ligands coordinated to the Fe(III) ion. In the second salt β''-$(BEDT\text{-}TTF)_5[Fe(C_5O_5)_3]\cdot C_6H_5CN$, the BEDT-TTF molecules are arranged in a β'' phase. The α-phase is a semiconductor with a high room-temperature conductivity (ca. 6 S cm^{-1} and an activation energy of 116 meV), whereas the β''-phase shows a high room-temperature conductivity (ca. 10 S cm^{-1}) and shows a metallic behavior from room temperature down to ca. 140 K, where an activated conductivity was observed. This type of behavior, although unusual, has already been observed in two related BEDT-TTF salts with the $[Ga(ox)_3]^{3-}$ anion, where an additional semiconductor−superconductor transition was observed at very low temperatures. As a progression of these studies, we report herein the synthesis, crystal structure, and physical properties of two new isostructural salts prepared by reacting the BDH-TTP (2,5-bis(1,3-dithiolan-2-ylidene)-1,3,4,6-tetrathiapentalene) organic donor (see Scheme 1), which is a BEDT-TTF isomer that contains no TTF moiety[13] with $[Fe(C_5O_5)_3]^{3-}$ and $[Ga(C_5O_5)_3]^{3-}$ (ref 14) anions.

Scheme 1. Molecular Structure of the Donor BDH-TTP

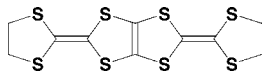

The BDH-TTP has been selected since it is expected to produce organic metals that retain the metal state down to low temperatures, as shown in Table 1. The aim of the present work is to investigate if any indirect interaction between the paramagnetic centers mediated by the π-electrons may influence the physical properties of the obtained salts.

EXPERIMENTAL SECTION

General Remarks. Single-crystal X-ray data were collected at low temperature on a Bruker AXS SMART-APEX/CCD area detector using graphite monochromated Mo Kα radiation (0.71079 Å). Since the crystal of compound **2** was very small, reflections in a 2θ range of 3.74°−46.00° were used for structure analysis. The structures were solved by direct methods using SIR97,[18] and structure refinements were carried out using full-matrix least-squares calculations (SHELXL-97).[18] Non-hydrogen atoms except for the solvent molecule were refined anisotropically, and the hydrogen atoms were treated using a riding model.

Synthesis of $(Bu_4N)_3[Fe(C_5O_5)_3]$ and $(Bu_4N)_3[Ga(C_5O_5)_3]$. The synthesis of the $(Bu_4N)_3[Fe(C_5O_5)_3]$ and $(Bu_4N)_3[Ga(C_5O_5)_3]$ were performed according to the literature.[19−21]

The cyclic voltammetry, made in CH_3CN in the range of 0.0−1.5 V, shows no oxidation or reduction peaks: for this reason, this complex was selected to be combined with BDH-TTP, which shows a monoelectronic reversible oxidation peak at 0.46 V.[13,19]

Synthesis of $(BDH\text{-}TTP)_6[Fe(C_5O_5)_3]\cdot CH_2Cl_2$ (1). Dark needle crystals of κ-$(BDH\text{-}TTP)_6[Fe(C_5O_5)_3]\cdot CH_2Cl_2$ (**1**) were grown by using the electrocrystallization method: BDH-TTP (3.5 mg) was dissolved in 10 mL of CH_2Cl_2, and the solution was placed in the anodic chamber of the cell. $(Bu_4N)_3[Fe(C_5O_5)_3]$ (33.4 mg, donor: anion molar ratio = 3:1) was dissolved in 15 mL of CH_2Cl_2, and this solution was divided into the anodic and cathodic compartments of the cell. A current density of 0.2 μA cm^{-2} was applied. Single crystals were grown at 25 °C on a platinum wire electrode for a period of 20 days. Crystallographic data for **1** are reported in Table 2.

Synthesis of $(BDH\text{-}TTP)_6[Ga(C_5O_5)_3]\cdot CH_2Cl_2$ (2). Brown crystals of κ-$(BDH\text{-}TTP)_6[Ga(C_5O_5)_3]\cdot CH_2Cl_2$ (**2**) were grown by using the electrocrystallization method: BDH-TTP (3.2 mg) was dissolved in 10 mL of CH_2Cl_2, and the solution was placed in the anodic chamber of the cell. $(Bu_4N)_3[Ga(C_5O_5)_3]$ (31.0 mg, donor: anion molar ratio = 3:1) was dissolved in 15 mL of CH_2Cl_2, and this solution was divided into the anodic and cathodic compartments of the cell. A current density of 0.2 μA cm^{-2} was applied. Single crystals were grown at 25 °C on a platinum wire electrode for a period of 20 days. Crystallographic data for **2** are reported in Table 2.

Conductivity. The electrical resistivity was measured using a four-terminal dc method with a measuring current of 0.1−0.01 mA. Four platinum wires were attached to a single crystal with carbon paste within the conducting plane. The measuring current was alternated in order to eliminate thermoelectric effects. The typical cooling rate was 1 K min^{-1}. The hydrostatic pressure was applied via Daphne 7373 oil with a BeCu pressure cell with an inner core of NiCrAl. The pressure was applied at room temperature, and the cell was clamped with screws. The pressure decreased by ca. 2 kbar at low temperatures, compared to that at room temperature.[19] The temperature was monitored with a calibrated Cernox thermometer.

ESR. The electron spin resonance (ESR) measurements were performed using a Bruker EMX X-band spectrometer equipped with an Oxford Model ESR900 gas flow cryostat for temperatures between room temperature and 5 K. A single crystal was fixed to a Teflon substrate with a small amount of Apiezon N grease. The absolute magnitude of the susceptibility and the g-value were calibrated using $CuSO_4\cdot 5H_2O$ and diphenylpicrylhydrazyl (DPPH) as standards, respectively.

Magnetic Measurements. The magnetic susceptibility measurements were carried out in the temperature range 2−300 K with an applied magnetic field of 0.1 T on a polycrystalline samples of compounds **1** and **2** (with masses of 6.53 and 3.18 mg, respectively) with a Quantum Design MPMS-XL-5 SQUID susceptometer. The susceptibility data were corrected for the sample holder previously measured using the same conditions and for the diamagnetic contributions of the salt, as deduced by using Pascal's constant tables. The isothermal magnetization was performed for compound **1** with the same sample at 2 K with magnetic fields up to 5 T.

RESULTS AND DISCUSSION

Crystal Structure of $(BDH\text{-}TTP)_6[M(C_5O_5)_3]\cdot CH_2Cl_2$, where M = Fe (1) and Ga (2). Both compounds **1** and **2** crystallize in the monoclinic crystal system with the space group

dx.doi.org/10.1021/ic302234j | Inorg. Chem. 2013, 52, 423−430

Table 1. Examples of κ-Phase Compounds Based on BDH-TTP

counterion	solvent	σ_{RT} [S cm^{-1}]	intradimer distance [Å]	interdimer dihedral angle [°]	ref
I_3^-	PhCl	230 (metallic T > 2.0 K)	n.a.	n.a.	13
$FeCl_4^-$	EtOH/PhCl	39 (metallic T > 1.5 K)	3.59	83.3	15
$[FeNO(CN)_5]^{2-}$	EtOH/$PhNO_2$	3.0−6.0 (metallic T > 4.2 K)	3.39 (**I**), 3.44 (**II**)	80.44	16
$[FeNO(CN)_5]^{2-}$	EtOH/$PhNO_2$	3.0−6.0 (metallic T > 4.2 K)	3.46	83.32	16
PF_6^-	TCE	102 (metallic T > 2.2 K)	3.53	82	13
$Hg_3Br_8^{2-}$	THF	40 (metallic T > 4.2 K)	3.58	83.3	17
1	CH_2Cl_2	10 (metallic T > 2.0 K, P > 7 kbar)	3.39 (**I**−**II**), 3.59 (**III**−**III***)	∼82.5	this work
2	CH_2Cl_2	10 (metallic T > 50 K, P > 7 kbar)	3.38 (**I**−**II**), 3.49(**III**−**III***)	∼82.5	this work

Table 2. Crystal Data for $(BDH\text{-}TTP)_6[Fe(C_5O_5)_3]\cdot CH_2Cl_2$ (1) and $(BDH\text{-}TTP)_6[Ga(C_5O_5)_3]\cdot CH_2Cl_2$ (2)

parameter	1	2
chemical formula	$C_{76}H_{50}Cl_2FeO_{15}S_{48}$	$C_{76}H_{50}Cl_2GaO_{15}S_{48}$
a (Å)	44.603(7)	44.006(7)
b (Å)	10.6036(2)	10.5748(2)
c(Å)	25.964(4)	26.171(4)
β (deg)	123.738(3)	123.807(3)
V (Å^3)	10211(3)	10120(3)
temp T (K)	100	100
Z	4	4
crystal system	monoclinic	monoclinic
space group	$C2/c$	$C2/c$
F(000)	5816	5836
μ Mo Kα (mm^{-1})	1.379	1.245
ωR_2	0.1366	0.0816
R_1	0.0633	0.0386

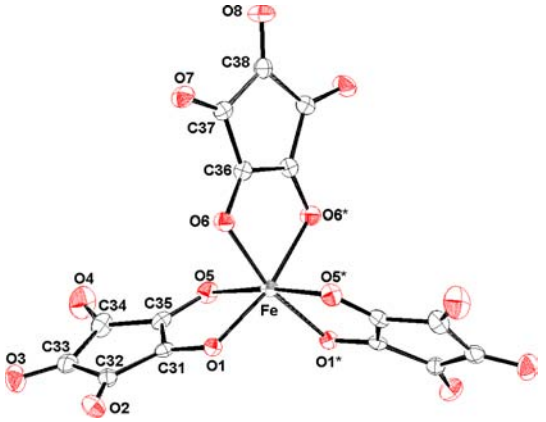

Figure 2. ORTEP drawing of $[Fe(C_5O_5)_3]^{3-}$ in compound **1** with the selected atom labeling scheme based on the unique atoms (50% probability ellipsoids). Symmetry operation (*): $-x + 2$, y, $-z + {}^1/_2$.

$C2/c$ and are crystallographically isostructural. The asymmetric units contains half $[M(C_5O_5)_3]^{3-}$ anion, located on a 2-fold axis, three BDH-TTP molecules and half CH_2Cl_2 co-crystallized solvent molecule. As a consequence of the presence of the 2-fold axis, two of the three croconato ligands are equivalent. Each ligand possesses a 2− charge to form $[M(C_5O_5)_3]^{3-}$ trianions with trivalent Fe or Ga. The labeling schemes for each BDH-TTP molecule and for the $[Fe(C_5O_5)_3]^{3-}$ anion are shown in Figures 1 and 2, respectively.

The structures of **1** and **2** consist of layers of BDH-TTP molecules separated by layers of isolated $[M(C_5O_5)_3]^{3-}$ complexes alternating along the a-axis, as shown in Figure 3. The organic layer is formed by three independent BDH-TTP molecules, (I, II, III), which present very similar bond distances and angles in both salts. The charge estimated for each molecule in both compounds, considering the length of the central-carbon double bond, is +0.5. Selected S−S distances for **1** and **2** are reported in Table 3, while S···S interactions shorter than the sum of the van der Waals radii in **1** are shown in

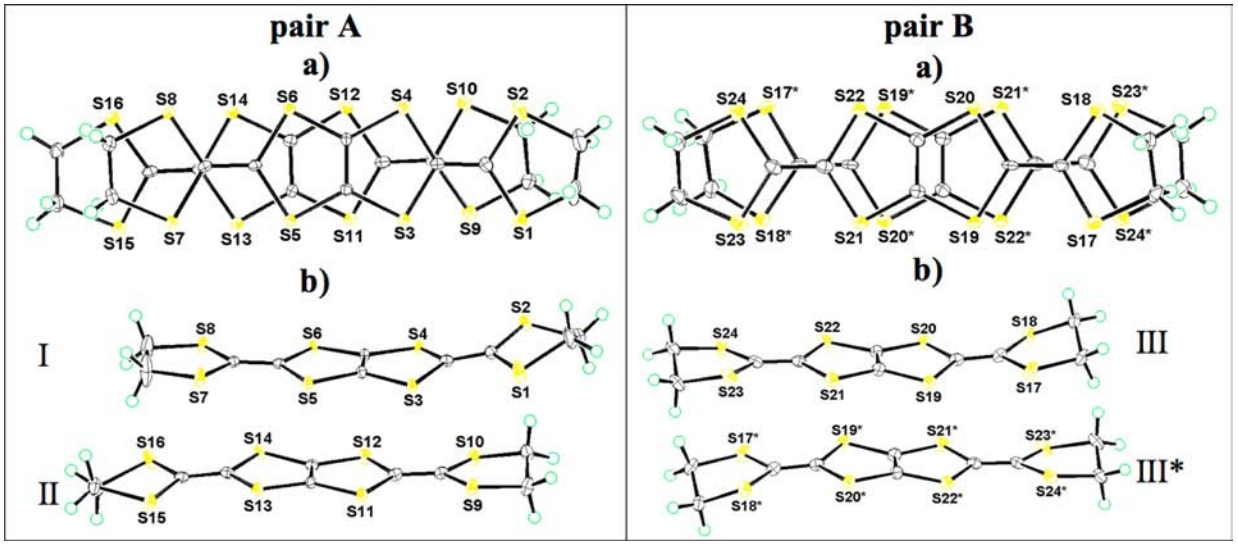

Figure 1. ORTEP drawing of the $(BDH\text{-}TTP)_2^+$ pairs (A, left) and (B, right) in compound **1** showing the atom labeling scheme (50% probability ellipsoids): (a) top view and (b) side view. Symmetry operation for pair B (*): $-x + {}^3/_2$, $-y - {}^3/_2$, $-z$.

dx.doi.org/10.1021/ic302234j | Inorg. Chem. 2013, 52, 423−430

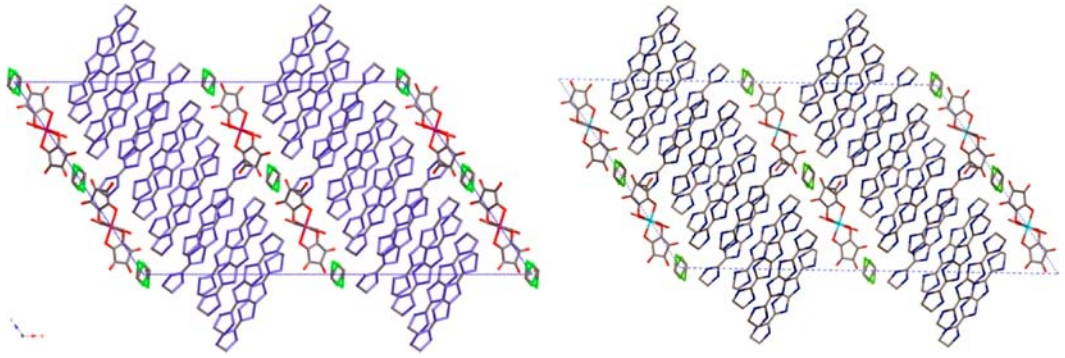

Figure 3. Molecular packing of (BDH-TTP)$_6$[Fe(C$_5$O$_5$)$_3$]·CH$_2$Cl$_2$ (**1**) (left) and (BDH-TTP)$_6$[Ga(C$_5$O$_5$)$_3$]·CH$_2$Cl$_2$ (**2**) (right). [H atoms have been omitted for clarity; color code: gray = C; red = O; blue = N; green = Cl.]

Table 3. Selected Bond Distances for Compounds 1 and 2[a]

bond	1	2
S16–S8	3.8810(1) Å	3.7607(2) Å
S8–S14	3.7011(1) Å	3.6286(2) Å
S14–S6	3.6411(1) Å	3.5992(2) Å
S6–S12	3.7202(1) Å	3.6936(2) Å
S12–S4	3.8051(1) Å	3.7544(2) Å
S4–S10	3.8218(1) Å	3.8182(2) Å
S10–S2	4.5881(1) Å	4.5360(2) Å
S15–S7	4.1137(1) Å	4.1747(2) Å
S7–S13	3.8346(1) Å	3.8867(2) Å
S13–S5	3.6363(1) Å	3.6184(18) Å
S5–S11	3.8103(1) Å	3.8028(2) Å
S11–S3	3.7552(1) Å	3.7277(2) Å
S3–S9	3.6274(1) Å	3.6275(2) Å
S9–S1	3.9726(1) Å	3.9600(2) Å
S24–S17*	3.8160(1) Å	3.7925(2) Å
S22–S17*	4.6677(1) Å	4.3168(2) Å
S22–S19*	3.5910(1) Å	3.5840(2) Å
S20–S19*	4.2468(1) Å	3.9571(2) Å
S20–S21*	3.6408(1) Å	3.6305(2) Å
S18–S21*	4.6648(1) Å	4.3542(2) Å
S18–S23*	4.0447(1) Å	3.9924(2) Å

[a]Symmetry transformations used to generate equivalent atoms: (*) $-x + {}^3/_2$, $-y - {}^3/_2$, $-z$.

Figure 4. These interactions, which are both, intradimers and interdimers, form a two-dimensional (2D) network in the *bc* plane. The three independent donor molecules are all distorted in one side, while the other side is almost coplanar with the TTP-moiety; in particular, molecules I show a strong bending in the 1,3-dithiolan-2-ylidene part, which contains the S1 and S2 atoms (see Figure 1 and Figure S1 in the Supporting Information).

Molecules I and II are dimerized to form a noncentrosymmetric pair A with shortest intradimer S···S contacts of 3.6363(1) and 3.5992(2) Å for **1** and **2**, respectively. Molecule III is also dimerized with molecule III* to form the pair B, the latter being related with the former by the symmetry operation of $(-x + {}^3/_2, -y - {}^3/_2, -z)$, with shortest intradimer contacts of 3.5910(1) and 3.5840(2) Å for **1** and **2**, respectively. The A- and B-type dimers are almost orthogonal (the interdimer angle is ca. 82.5°), leading to a κ-type molecular packing in both compounds, as shown in Figure 4. In both salts, each B-type dimer is surrounded by six A dimers. Inside these A-type dimers, the distances between the planes calculated considering the TTP moiety are 3.39 and 3.38 Å for the iron and the gallium salt, respectively, whereas in the B-type pair, these distances are 3.59 and 3.49 Å for **1** and **2**, respectively (Table 1). A comparison with others BDH-TTP salts showing the same κ-phase is reported in Table 1. As can be seen in Table 1, compounds **1** and **2** exhibit similar interdimer dihedral angles. The presence of two crystallographically independent dimers with similar interplanar distances and dihedral angles is also observed in other BDH-TTP salts as (BDH-TTP)$_4$[FeNO(CN)$_5$]·PhNO$_2$,[16] and (BDH-TTP)$_4$Hg$_3$Br$_8$.[17]

The anionic layer is formed by isolated [M(C$_5$O$_5$)$_3$]$^{3-}$ units and solvent molecules. The M(III) ions are surrounded by three croconato ligands acting as 1,2-bidentate. The [M(C$_5$O$_5$)$_3$]$^{3-}$ anions are arranged in two rows, each one formed only by Λ or Δ enantiomers, as shown in Figure 5. The presence of both enantiomers in equal amounts leads to achiral compounds, as previously observed for similar compounds based on [Fe(C$_5$O$_5$)$_3$]$^{3-}$.[7]

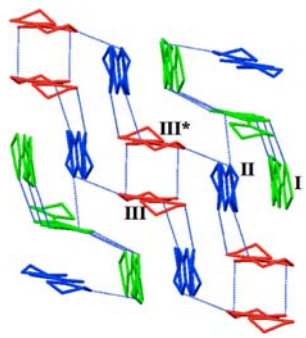

Figure 4. Molecular packing of BDH-TTP in compound **1** (κ-type); short S···S contacts are indicated by dashed lines.

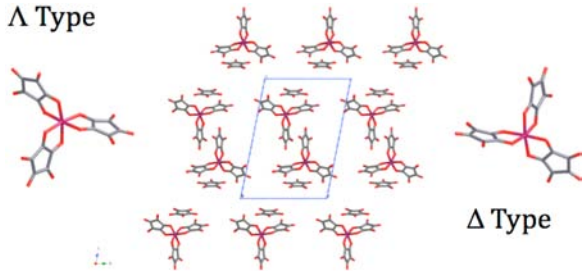

Figure 5. The Λ and Δ enantiomers rows in the packing of [Ga(C$_5$O$_5$)$_3$]$^{3-}$ in compound **2**.

dx.doi.org/10.1021/ic302234j | Inorg. Chem. 2013, 52, 423–430

Physical Properties. Electronic Structure. The κ-type arrangement with orthogonal dimers of BDH-TTP molecules in a conducting plane and the labeling of transfer integrals between them are shown in Figure 6. The charge of BDH-TTP

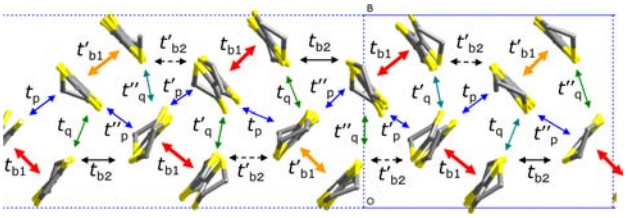

Figure 6. κ-type donor arrangement in a conducting plane with overlap integrals between molecules.

seems to be uniform considering the length of the central-carbon double-bond. The overlap integrals between HOMOs calculated on the basis of the extended Hückel model[22] are shown in Table 4. The overlap integrals between dimerized

Table 4. Overlap Integrals for M = Fe and M = Ga Salts

	Overlap Integrals (× 10^{-3})	
	M = Fe	M = Ga
t_{b1}	21.6	22.8
t'_{b1}	21.4	20.7
t_{b2}	13.1	12.9
t'_{b2}	13.9	14.5
t_p	5.5	5.5
t'_p	7.0	7.4
t''_p	11.6	9.3
t_q	−0.91	−0.26

molecules are twice as large as the other integrals. Values for **1** are almost the same as for **2**. Intermolecular contacts in the κ-type packing are shorter than the sum of the van der Waals radii, as shown in Figure 4.

Transport Properties. The resistivity measurements for **1** and **2** have been performed from ambient pressure up to 15 kbar. At ambient pressure, the conductivity is 12 S cm^{-1} for **1** and **2** (see Figures S2a and S2b, respectively, in the Supporting Information); the resistivity of each salt shows a thermal hysteresis on the temperature sweep direction indicated by small arrows and such hysteresis may be caused by microcracks during initial cooling as often observed for organic conductors. Increasing the pressure (4 kbar), the room-temperature conductivity is ca. 10 S cm^{-1} for **1** and **2** but the metal−insulator transition is still observed. The temperature dependences of the resistivity under pressures of up to 15 kbar for **1** and **2** are shown in Figures 7a and 7b, respectively. Both salts exhibit metallic behavior from room temperature down to ca. 100 K; below this temperature, the conductivity becomes thermally activated with a typical activation energy of 1−2 meV. These behaviors are similar to those previously reported for the α and β″ salts obtained with BEDT-TTF and the $[Fe(C_5O_5)_3]^{3-}$ anion.[7] Under applied pressure, the metal−semiconductor transition is suppressed at 7 kbar, as shown in Figure 7a. For the M = Ga salt (**2**), the metal−semiconductor transition is still observed even at applied pressures of 15 kbar (Figure 7b).

Magnetic Measurements for (1). The thermal variation of the product of the molar magnetic susceptibility per Fe(III)

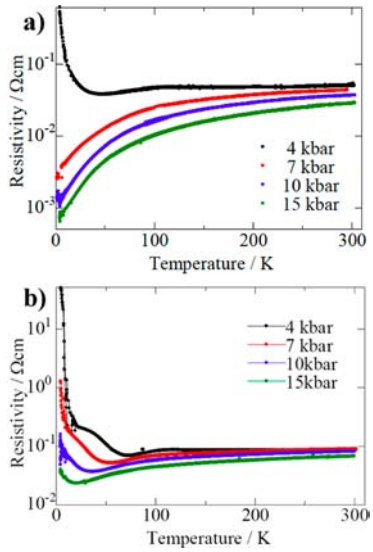

Figure 7. Temperature dependence of the electrical resistivity under applied pressure for (a) compound **1** and (b) compound **2**.

ion times the temperature ($\chi_m T$) shows, at room temperature, a value of ca. 5.0 cm^3 K mol^{-1} (Figure 8), close to that reported

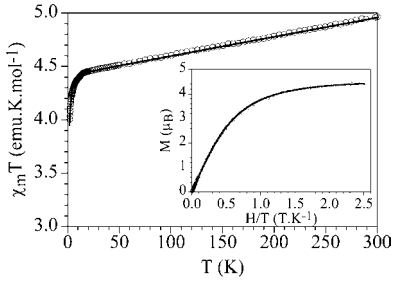

Figure 8. Thermal variation of the $\chi_m T$ product for compound **1**. Inset shows the isothermal magnetization at 2 K. Solid lines are the best fit to the models (see text).

in the literature for the metallic salt of BEDT-TTF with the same anion: β″-$(BEDT\text{-}TTF)_5[Fe(C_5O_5)_3]\cdot PhCN$ (5.2 cm^3 K mol^{-1})[7] and above the values reported for the semiconducting salt α-$(BEDT\text{-}TTF)_5[Fe(C_5O_5)_3]\cdot 5H_2O$ (ca. 4.5 cm^3 K mol^{-1})[7] and the Bu_4N^+ and Ph_4P^+ salts of the same anion (ca. 4.5 and 4.6 cm^3 K mol^{-1}, respectively).[23] When the temperature is decreased, the $\chi_m T$ value shows a linear decrease to reach a value of ca. 4.5 cm^3 K mol^{-1} at ca. 20 K and a sharp decrease at lower temperatures, reaching a value of ca. 3.9 cm^3 K mol^{-1} at 2 K. The linear decrease observed in $\chi_m T$ product can be ascribed to the presence of a Pauli paramagnetism, typical of metallic systems and the sharp decrease observed at very low temperatures is ascribed to the presence of a zero field splitting (ZFS) of the $S = {}^5/_2$ high spin Fe(III) ion. Accordingly, the magnetic data of **1** were fit with a simple isolated monomer model for an $S = {}^5/_2$ high spin Fe(III) ion with a ZFS plus a temperature-independent paramagnetism (Nα). This simple model reproduces, very satisfactorily, the magnetic properties of **1** in the entire temperature range with $g = 2.010$, $|D| = 0.95$ cm^{-1}, and $N\alpha = 1.8 \times 10^{-3}$ cm^3 mol^{-1} (solid line in Figure 8). Note that (i) the sign of D cannot be determined from magnetic measurements on a powder sample and (ii) the D value could include a very weak antiferromagnetic coupling between the Fe(III) ions. The value obtained for

dx.doi.org/10.1021/ic302234j | Inorg. Chem. 2013, 52, 423−430

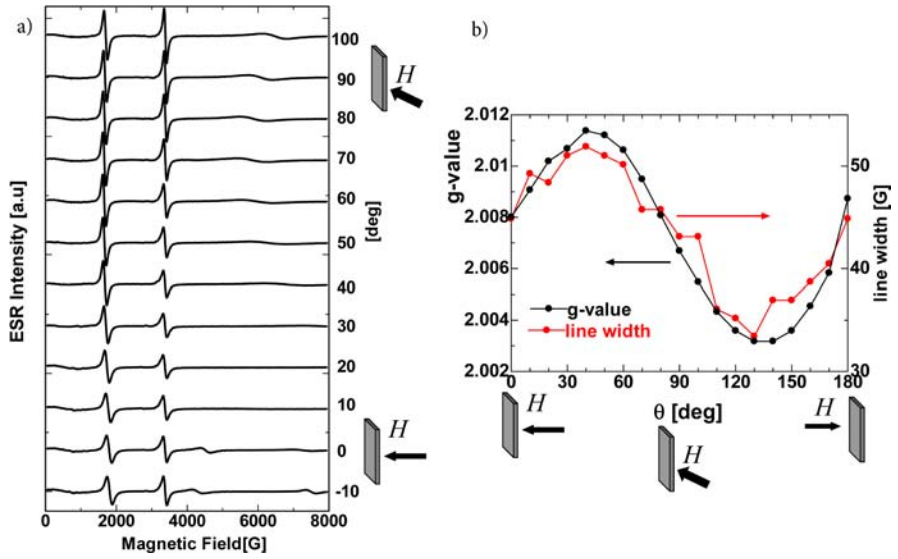

Figure 9. (a) Angular dependence of the ESR spectra of compound **1**. (b) Angular dependence of the *g*-factor and linewidth for compound **2**.

the Pauli paramagnetism is within the normal range observed for other molecular metals.[19] The isothermal magnetization confirms the paramagnetic behavior of **1** (inset in Figure 8). Thus, it shows a saturation value slightly below 5 μ_B and can be well reproduced with a Brillouin function for an $S = {}^5/_2$ ion, although with a reduced *g*-value due to the lower magnetic moment observed at low temperatures, as a consequence of the ZFS of the Fe(III) ion.

As expected, **2** is diamagnetic and shows a very low Pauli-type paramagnetism with a weak Curie-type contribution at low temperatures.

ESR. The ESR spectra of the two salts at room temperature, as a function of the angle between the magnetic field and the conducting plane, are shown in Figure 9. The ESR spectrum of **1**, besides the signal at $g \approx 2.00$, probably originated from the π-electrons of the BDH-TTP donors, shows a sharp feature at ca. 1800 G and broad ones at 500 G, 4500 G, and 7200 G. When the external field was rotated with respect to the conducting plane, these signals exhibited angle dependence. These signals are interpreted as caused by the fine structure splitting of the high-spin ($S = {}^5/_2$) state of Fe(III) in the distorted octahedral crystal field from the ligands.[24] As expected, the ESR spectrum of compound **2** only shows the signal attributed to the π-electron (Figure 9b), since it contains the diamagnetic $[Ga(C_5O_5)_3]^{3-}$ anion. When the external field was rotated with respect to the conducting plane, the *g*-value and linewidth changed, in the ranges of 2.003−2.011 and 34−52 G, respectively.

The temperature dependence of the spin susceptibility for the π-electrons in **1**, obtained by twice integrating the ESR signal at $g \approx 2.00$, is shown in Figure 10a. The spin susceptibility is Pauli-like above ca. 50 K, in agreement with the static magnetic susceptibility measurements (see above). Below ca. 50 K it shows an increase to reach a maximum at ca. 30 K followed by a sharp decrease at lower temperatures, in parallel with the decrease observed in the *g*-value and the divergence in the linewidth (Figure 10b). These behaviors are consistent with the metallic state at high temperature and the insulating phase at low temperature. The suppression of the π-electron signal below 20 K may be caused by the presence of antiferromagnetic exchange interactions within the donor layer.

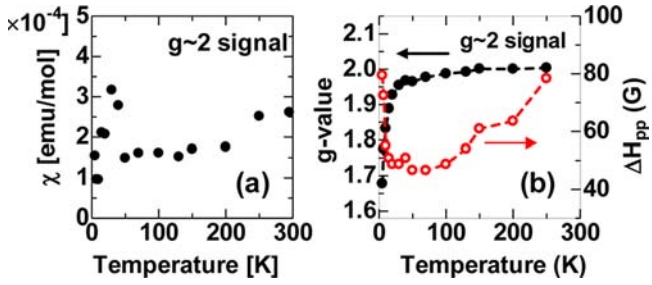

Figure 10. Temperature dependence of (a) the spin susceptibility and (b) *g*-value and linewidth for the π-electrons of compound **1** when the magnetic field is parallel to the conducting plane.

Note that this possible coupling cannot be observed in the SQUID measurements since the Fe(III) signal masks the contribution of the π-electrons. On the other hand, the ESR intensity of the Fe(III) signals increased, obeying the Curie law with decreasing temperature, also in agreement with the magnetic susceptibility measurements.

The temperature dependence of the spin susceptibility for salt **2** shows a Lorentzian line shape and a Pauli-like susceptibility above 100 K (Figure 11), indicative of a metallic state. Below 100 K, the spin susceptibility shows a Curie-like behavior with a Curie constant of ca. 2.9×10^{-3} cm^3 K mol^{-1},

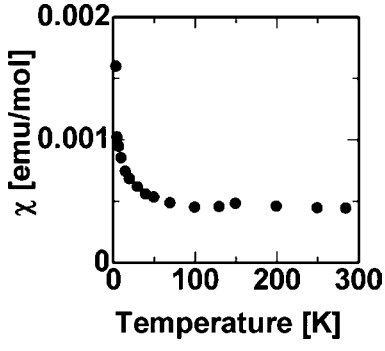

Figure 11. Temperature dependence of the spin susceptibility of compound **2** salt under magnetic field applied perpendicular to the conducting plane.

dx.doi.org/10.1021/ic302234j | *Inorg. Chem.* 2013, 52, 423−430

originating from defect sites with a concentration of one spin per 400 dimers. This is also confirmed from the fact that the ESR signal became asymmetric with a Gaussian line shape below 50 K.

CONCLUSIONS

Two new isostructural molecular metals—(BDH-TTP)$_6$[Fe(C$_5$O$_5$)$_3$]·CH$_2$Cl$_2$ (**1**) and (BDH-TTP)$_6$[Ga(C$_5$O$_5$)$_3$]·CH$_2$Cl$_2$ (**2**)—have been prepared and fully characterized. By comparing the magnetic properties of these two compounds, it has been possible to investigate the magnetic contribution of both networks, since, in **2**, the EPR measurements only show the contribution of the organic donor. Conductivity measurements show that these two materials behave as metals with rather high conductivity values (~10 S cm^{-1} for both compounds) at room temperature. The conductivity increases when the applied pressure is increased and, furthermore, in **1**, the metal−insulator transition observed at low temperatures and ambient pressure is suppressed above 7 kbar to show a metallic behavior down to low temperatures. **2** does not show the suppression of the M-I transition, although, as in compound **1**, the M-I transition is shifted toward lower temperatures and, most probably, pressures above 15 kbar are expected to suppress the M-I transition, as observed in compound **1** above 7 kbar. Static magnetic measurements show that compound **1** is a paramagnet with a Pauli paramagnetism of ca. 1.8 × 10^{-3} cm^3 mol^{-1}, typical of metallic systems, and a ZFS of 0.95 cm^{-1} in the high spin $S = {}^5/_2$ Fe(III) ions, in agreement with the structure. The spin susceptibility behavior is Pauli-like above ca. 50 K, in agreement with the static magnetic susceptibility measurements and is consistent with the metallic state at high temperature and the insulating phase at low temperature. The suppression of the π-electron signal below 20 K may be caused by the presence of antiferromagnetic exchange interactions within the donor layer. Note that this possible coupling cannot be observed in the SQUID measurements since the Fe(III) signal mask the contribution of the π-electrons. As a result of the lack of close anion−cation interactions, the two sublattices behave independently and any π-d interaction has been detected.

ASSOCIATED CONTENT

Supporting Information

This material is available free of charge via the Internet at http://pubs.acs.org.

AUTHOR INFORMATION

Corresponding Author

*Tel.: +39 070 6754486. Fax: +39 070 6754456. E-mail: mercuri@unica.it.

Notes

The authors declare no competing financial interest.

ACKNOWLEDGMENTS

INSTM, Regione Autonoma della Sardegna, L.R. 7-8-2007, Bando 2009, CRP-17453 Project "*Nano Materiali Multifunzionali per Applicazioni nell'Elettronica Molecolare*", the Spanish Ministerio de Economía y Competitividad (Consolider-Ingenio in Molecular Nanoscience Project Nos. CSD2007-00010 and CTQ-2011-26507), the Generalitat Valenciana (Programs Prometeo2009/095 and ISIC) and EU Marie Curie programme (for LP) are acknowledged for funding.

REFERENCES

(1) Day, P.; Coronado, E. *Chem. Rev.* **2004**, *104*, 5419 and references therein.

(2) (a) Gudenko, A. V.; Ginodman, V. B.; Korotkov, V. E.; Koshelap, A. V.; Kushch, N. D.; Laukhin, V. N.; Rozenberg, L. P.; Khomenko, A. G.; Shibaeva, R. P.; Yagubskii, E. B. In *The Physics and Chemistry of Organic Superconductors*; Saito, G., Kagoshima, G., Eds.; Springer−Verlag: Berlin, 1990. (b) Kurmoo, M.; Mallah, T.; Marsden, L.; Allan, M.; Friend, R. H.; Pratt, F. L.; Hayes, W.; Chasseau, D.; Bravic, G.; Duchase, L.; Day, P. *J. Am. Chem. Soc.* **1992**, *114*, 10722.

(3) Coronado, E.; Falvello, L. R.; Galán-Mascarós, J. R.; Giménez-Saiz, C.; Gómez-García, C. .J; Lauhkin, V. N.; Pérez-Benítez, A.; Rovira, C.; Veciana, J. *Adv. Mater.* **1997**, *9*, 984.

(4) Yamaguchi, K.; Kitagawa, Y.; Onishi, T.; Isobe, H.; Kawakami, T.; Nagao, H.; Takamizawa, S. *Coord. Chem. Rev.* **2002**, *226*, 235 and references therein.

(5) (a) Goze, F.; Laukhin, V. N.; Brossard, L.; Audouard, A.; Ulmet, J. P.; Askenazy, S.; Naito, T.; Kobayashi, H.; Kobayashi, A.; Tokumoto, M.; Cassoux, P. *Europhys. Lett.* **1994**, *28* (6), 427. (b) Balicas, L.; Brooks, J. S.; Storr, K.; Uji, S.; Tokumoto, M.; Tanaka, H.; Kobayashi, H.; Kobayashi, A.; Barzykin, V.; Gor'kov, L. P. *Phys. Rev. Lett.* **2001**, *87*, 067002-1.

(6) (a) Coronado, E.; Curreli, S.; Giménez-Saiz, C.; Gómez-García, C. J. *J. Mater. Chem.* **2005**, *15*, 1429. (b) Coronado, E.; Curreli, S.; Giménez-Saiz, C.; Gómez-García, C. J. *Inorg. Chem.* **2012**, *51*, 1111.

(7) (a) Mercuri, M. L., Deplano, P., Serpe, A., Artizzu, F. Multifunctional Materials of Interest in Molecular Electronics. In *Handbook of Multifunctional Molecular Materials*; Ouahab, L., Ed.; Pan Stanford Publishing: Singapore, 2012 (in press). (ISBN: 9789814364294.) (b) Coronado, E.; Curreli, S.; Giménez-Saiz, C.; Gómez-García, C. J.; Deplano, P.; Mercuri, M. L.; Serpe, A.; Pilia, L.; Faulmann, C.; Canadell, E. *Inorg. Chem.* **2007**, *46*, 4446. (c) Gómez-García, C. J.; Coronado, E.; Curreli, S.; Giménez-Saiz, C.; Deplano, P.; Mercuri, M. L.; Pilia, L.; Serpe, A.; Faulmann, C.; Canadell, E. *Chem. Commun.* **2006**, 4931.

(8) (a) Castro, I.; Faus, J.; Julve, M.; Journaux, Y.; Sletten, J. *J. Chem. Soc., Dalton Trans.* **1991**, 2533. (b) Castro, I.; Faus, J.; Julve, M.; Mollar, M.; Monge, A.; Gutiérrez-Puebla, E. *Inorg. Chim. Acta* **1989**, *161*, 97.

(9) Castro, I.; Calatayud, M. L.; Lloret, F.; Sletten, J.; Julve, M. *J. Chem. Soc., Dalton Trans.* **2002**, 2397.

(10) (a) Castan, P.; Deguenon, D. *Acta Crystallogr., Sect. C: Cryst. Struct. Commun.* **1991**, *47*, 2656. (b) Carranza, J.; Sletten, J.; Brennn, C.; Lloret, F.; Cano, J.; Julve, M. *Dalton Trans.* **2004**, 3997. (c) Wang, C.-C.; Yang, C.-H.; Lee, G.-H. *Inorg. Chem.* **2002**, *41*, 1015. (d) Gavilan, E.; Audebrand, N. *Polyhedron* **2007**, *26*, 5533.

(11) (a) Castro, I.; Sletten, J.; Faus, J.; Julve, M.; Journaux, Y.; Lloret, F.; Alvarez, S. *Inorg. Chem.* **1992**, *31*, 1889. (b) Speier, G.; Speier, E.; Noll, B.; Pierpont, C. G. *Inorg. Chem.* **1997**, *36*, 1520. (c) Plater, M. J.; Foreman, M. R. St. J.; Howie, R. A. *J. Chem. Crystallogr.* **1998**, *28*, 653. (d) Wang, C.-C.; Tseng, S.-M.; Lin, S.-Y.; Liu, F.-C.; Dai, S.-C.; Lee, G.-H.; Shih, W.-J.; Sheu, H.-H. *Cryst. Growth Des.* **2007**, *7*, 1783. (e) Abbati, G. L.; Cornia, A.; Babretti, A. C. *Acta Crystallogr., Sect. C: Cryst. Struct. Commun.* **1999**, *55*, 2043. (f) Wang, C.-C.; Yang, C.-H.; Tseng, S.-M.; Lee, G.-H.; Chiang, Y.-P.; Sheu, H.-S. *Inorg. Chem.* **2003**, *42*, 8294. (g) Cornia, A.; Fabretti, A. C.; Giusti, A.; Ferraro, F.; Gatteschi, D. *Inorg. Chim. Acta* **1993**, *212*, 87. (h) Ghoshal, D.; Ghosh, A. K.; Ribas, J.; Mostafa, G.; Chaudhuri, N. R. *Cryst. Eng. Commun.* **2005**, *7*, 616. (i) Brouca-Cabarrecq, C.; Trombe, J. C. *Inorg. Chim. Acta* **1992**, *191*, 227. (l) de Paula, E. E. B.; Visentin, L. C.; Yoshida, M. I.; De Oliveira, L. F. C.; Machado, F. C. *Polyhedron* **2011**, *30*, 213. (m) Atzori, M.; Sessini, E.; Artizzu, F.; Pilia, L.; Serpe, A.; Gómez-García, C. J.; Giménez-Saiz, C.; Deplano, P.; Mercuri, M. L. *Inorg. Chem.* **2012**, *51* (9), 5360−5367.

(12) (a) Wang, C.-C.; Kuo, C.-T.; Yang, J.-C.; Lee, G.-H.; Shih, W.-J.; Sheu, H.-S. *Cryst. Growth Des.* **2007**, *7*, 1476. (b) Gavilan, E.; Audebrand, N. *Polyhedron* **2007**, *26*, 5533. (c) Maji, T. K.; Konar, S.; Mostafa, G.; Zangrando, E.; Lu, T.-H.; Chaudhuri, N. R. *J. Chem. Soc., Dalton Trans.* **2003**, 171.

(13) Yamada, J.-I.; Watanabe, M.; Anzai, H.; Nishikawa, H.; Ikemoto, I.; Kikuchi, K. *Angew. Chem., Int. Ed.* **1999**, *38* (6), 810.
(14) Mercuri, M. L.; Deplano, P.; Pilia, L.; Serpe, A.; Marchiò, L.; Bernot, K.; Artizzu, F. *Inorg. Chim. Acta* **2011**, *370*, 474.
(15) Kikuchi, K.; Nishikawa, H.; Ikemoto, I.; Toita, T.; Akutsu, H.; Nakatsuji, S.; Yamada, J. *J. Solid State Chem.* **2002**, *168*, 503.
(16) Shevyakova, I.; Buravov, L.; Tkacheva, V.; Zorina, L.; Khasanov, S.; Simonov, S.; Yamada, J.; Canadell, E.; Shibaeva, R.; Yagubskii, E. *Adv. Funct. Mater.* **2004**, *14* (7), 660.
(17) Zhilyaeva, E. I.; Flakina, A. M.; Lyubovskaya, R. N.; Fedyanin, I. V.; Lyssenko, K. A.; Antipin, M. Yu.; Lyubovskii, R. B.; Yudanova, E. I.; Yamadac, J. *Synth. Met.* **2006**, *156*, 991.
(18) *SHELXTL-PC Package*; Bruker AXS, Inc.: Madison, WI, USA, 1998.
(19) Williams, J. M. J. R.; Thorn, J.; Carlson, K. D.; Geiger, U.; Wang, H. H.; Kini, A. M.; Whangbo, M. H. In *Organic Superconductors: Synthesis, Structure, Properties and Theory*; Crimes, R. N., Ed.; Prentice Hall: Englewood Cliffs, NJ, 1992.
(20) Kushch, N. D.; Kazakova, A. V.; Buravov, L. I.; Yagubskii, E. B.; Simonov, S. V.; Zorina, L. V.; Khasanov, S. S.; Shibaeva, R. P.; Yamada, J.; Umemiyac, M. *Russ. Chem. Bull., Int. Ed.* **2010**, *59* (9), 1729.
(21) Artizzu, F.; Deplano, P.; Pilia, L.; Serpe, A.; Marchiò, L.; Bernot, K.; Mercuri, M. L. *Inorg. Chim. Acta* **2011**, *370*, 474.
(22) Mori, T.; Kobayashi, A.; Sasaki, Y.; Kobayashi, H.; Saito, G.; Inokuchi, H. *Bull. Chem. Soc. Jpn.* **1984**, *57*, 627.
(23) Curreli, S.; Deplano, P.; Faulmann, C.; Mercuri, M. L.; Pilia, L.; Serpe, A.; Coronado, E.; Gómez-Garcia, C. J. *Inorg. Chim. Acta* **2006**, *359*, 1177.
(24) Coronado, E.; Curreli, S.; Giménez-Saiz, C.; Gómez-Garcia, C. J.; Alberola, A. *Inorg. Chem.* **2006**, *45*, 10815.